ICAS 2021 SHANGHAI
International Council of the Aeronautical Sciences
32nd Congress of the International Council of the Aeronautical Sciences
September 6-10, 2021
Pudong Shangri-La, Shanghai, China

# Effect of Droplet MVD on Icing Collection Efficiency for a Helicopter Blade

Weibin Li[1], Kaicheng Li[2], Chao Song[1], Honglin Ma[1] & Yingyu Wang[1]

[1] Computational Aerodynamics Institute, China Aerodynamics Research and Development Center, Mianyang, 621000, China
[2] China Helicopter Research and Development Institute, Aviation Industry Corporation of China, Jingdezhen, 333001, China

## Abstract

The helicopter is an indispensable power to carry out tasks in alpine regions. The cold weather is an enormous challenge for the helicopter, which may cause blade-icing problems. In order to study the effect of droplet mean volume diameter (MVD) on icing range, comparisons about droplet collection efficiency under different MVDs are presented in this paper. Firstly, based on multi-reference coordinate systems and the SIMPLE algorithm, a computational method for airflow field with the structured grid is established. Secondly, the Euler method is applied to the simulation of droplets motions and the corresponding computational method of droplet collection efficiency is proposed. Finally, collection efficiency at different sections of the blade and the coverage range of droplets under different MVDs are presented and analyzed. The paper can provide qualitative results of the icing trend affected by MVDs, and may provide numerical supports for helicopter anti-icing.

**Keywords:** droplet collection efficiency; helicopter blade icing; multi-reference coordinate system; Euler method

## 1. Introduction

The helicopter is required to carry out tasks in alpine regions and it must have the ability of long-time flight, which makes helicopters often encounter severe weather during their missions, such as rain, snow, and frost. When the content of cooled droplets in the atmosphere reaches a certain level, icing may be formed on the key components, blades and engines, of a helicopter. Icing may cause helicopter vibration, rotor lift reduction, and engine power shortage, even a crash accident [1]. Therefore, it is an important issue to consider the helicopter icing and anti-icing in its design process.

The real icing environment is difficult to be produced in icing test, and the flight of icing test is expensive and its safety is not easy to be guaranteed [2, 3, 4]. Due to these reasons, numerical simulation has become one of the most important means of helicopter icing and anti-icing prediction.

The droplet collection efficiency is the key element in numerical simulation of icing, it can show how serious the icing happened and give input for ice accretion prediction. There are two common means to compute the droplet collection efficiency, the Lagrangian and Eulerian two-phase flow methods [5]. Among them, the Eulerian method is more widely used because of its high computational efficiency. It has been applied to complex shapes, mainly to verify the similarity theory, evaluate the icing severity, and predict the thermal load of a deicing system [6, 7]. The Euler method has been developed for several decades and its accuracy has also been verified.

For rotating parts, the droplet collection efficiency of aero-engine rotating fairing, aero-engine rotating surface, and wind turbine blades has been carried out by the Euler method, and its influence law of icing conditions is analyzed [8-10]. And for the rotor of helicopter, there are many kinds of researches about icing, including the numerical simulation method of rotor icing and the influence of rotor icing on aerodynamic performance. The commercial software, FENSAP [11], has added the numerical simulation function of rotor icing. However, most numerical simulations still use the methods for the non-rotating situation. Concretely, the rotor is segmented into several parts and the icing simulation is carried out on the two-dimensional cross-section or the segment [12, 13]. And then the icing of the rotor is approximated by the results at different positions. In recent years, the analysis of droplet imp-

-act and collection characteristics based on rotating coordinate system has also been carried out, which improves the simulation accuracy of rotating icing.

In rotor icing, the average size of droplets is an important factor that may affect the icing intensity [14]. In order to get a clear understanding of how the droplet size works, a collection efficiency calculation method by multiple reference frame (MRF) is given and the droplet impact characteristics of a rotor are studied in this paper. The method employs the classical SIMPLE algorithm and the Euler method to establish the solution of governing equation for droplets. And the influence of the mean volume diameter (MVD) of water droplets on the collection efficiency of the blade is discussed in the numerical experiment part.

The remainder of this paper is organized as follows. In Section 2, we give a briefly introduction of our method for airflow and droplet. In Section 3, the computational mesh and the result of collection efficiency are discussed. At last, the conclusion is shown in section 4.

## 2. Governing equations

Due to the small size of the droplets, it is assumed that the droplets have no reaction on the air when calculating the movement and impact characteristics of the droplets. Therefore, the calculating of motion process of water droplets is divided into two steps. Firstly, calculate the airflow field and obtain the flow field information including velocity at different positions in the space. Secondly, calculate the water droplets trajectories, and obtain the impacting area and intensity of the droplets on the blade surface.

### 2.1 Governing equations for airflow

The multi reference frame (MRF) method is used to calculate the airflow field. The main idea is to divide the calculation region into non-rotating and rotating parts. In the non-rotating region, the regular Navier-Stokes equations are solved. In the rotating region, the Coriolis force and centrifugal force are introduced as body forces, and the following control equations are determined:

$$\frac{\partial \rho_a}{\partial t} + \nabla \cdot (\rho_a \vec{u_r}) = 0 \tag{1}$$

$$\frac{\partial (\rho_a \vec{u_r})}{\partial t} + \nabla \cdot (\rho_a \vec{u_r} \vec{u_r}) + \rho_a [2\vec{\omega} \times \vec{u_r} + \vec{\omega} \times (\vec{\omega} \times \vec{r})] = -\nabla p + \nabla \cdot \tau_r + \vec{F} \tag{2}$$

where $\rho_a$ is the air density, $p$ is the pressure, $\tau_r$ is the viscous stress, $\vec{F}$ is the external force, $\vec{\omega}$ is the rotation angular velocity, $\vec{r}$ is the vector diameter of the control body under the rotation system, and $\vec{u_r}$ is the relative air velocity with the following form:

$$\vec{u_r} = \vec{u} - \vec{\omega} \times \vec{r} \tag{3}$$

where $\vec{u}$ is the absolute air speed.

In Eqs. (1) and (2), the convection term and the source term are discretized by the finite volume method, the first term is discretized by the second-order implicit method, and the pressure is calculated by the SIMPLE method.

### 2.2 Solution of droplet collection efficiency

The Euler method is used to calculate the movement and collection of water droplets. The discrete droplets are regarded as a continuous phase by the Euler method, and the volume fraction is introduced to control the volume proportion of droplets in the body. Similarly, the influence of Coriolis force should also be considered in the calculation of water phase. The motion equation of water droplet in the rotating system is as follows:

$$\frac{\partial (\rho \alpha)}{\partial t} + \nabla \cdot (\rho \alpha \vec{u_r}) = 0 \tag{4}$$

$$\frac{\partial(\rho\alpha\overrightarrow{u_{dr}})}{\partial t}+\nabla\cdot(\rho\alpha\overrightarrow{u_{dr}}\overrightarrow{u_{dr}})+\rho\alpha[2\vec{\omega}\times\overrightarrow{u_{dr}}+\vec{\omega}\times(\vec{\omega}\times\vec{r})]=\rho\alpha K(\overrightarrow{u_r}-\overrightarrow{u_{dr}}) \tag{5}$$

where $\alpha$ is the volume fraction of water drop, $\rho$ is the density of water drop, $\overrightarrow{u_{dr}}$ is the relative speed of water drop, and $K$ is the inertia factor [2] with the following form:

$$K=\frac{18\mu_a}{\rho d^2}\cdot\frac{C_D\,\mathrm{Re}}{24} \tag{6}$$

where $\mu_a$ is the air viscosity, $d$ is the droplet diameter, $C_D$ is the resistance coefficient, and $\mathrm{Re}$ is the relative Reynolds number.

The discretization method for Eqs. (4) and (5) is still chosen as the finite volume method, and the first term is discretized by the first-order explicit method.

The boundary condition of the blade surface is set as escape (outlet) where droplets will be stuck here. And the drop collection efficiency is determined by the following formula:

$$\beta=\frac{\alpha}{\alpha_\infty}\frac{\left|\overrightarrow{u_{dr}}\cdot\vec{n}\right|}{\left|\overrightarrow{u_\infty}\right|} \tag{7}$$

where $\vec{n}$ is the normal vector of the surface grid, $\alpha_\infty$ and $\overrightarrow{u_\infty}$ are the volume fraction and velocity of water droplets given at the inlet, respectively.

## 3. Results and analysis

### 3.1 Computational mesh

A certain type of rotor is selected for the calculation. The radius of rotation is about 15 meters, the direction of far-field flow is X-axis, the vertical direction of the rotor is Z-axis, and the Y-axis is determined by the right-hand rule. The structured mesh with multi blocks is used to generate the grid, and the amount of grids is about 60 million. In Fig. 1, the partition of rotating region and the grids near the blade surface are given. In this computation, the grids near the blade surface are refined to improve the calculation accuracy.

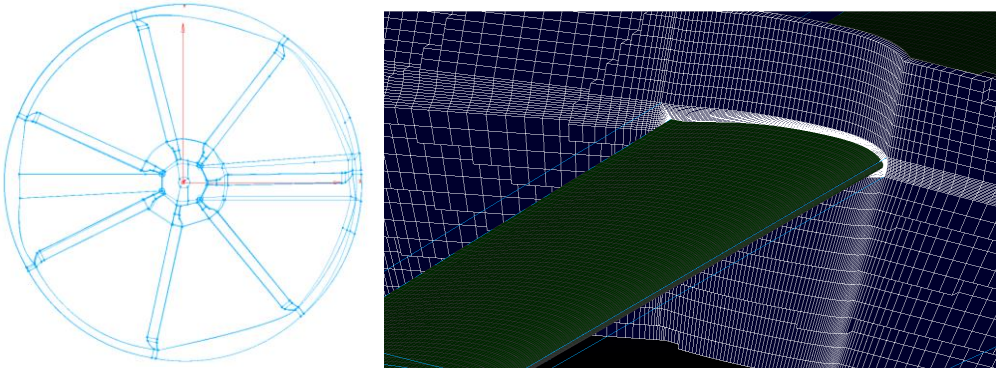

(a) (b)

Figure 1 – Partition of rotating region and grids near the surface of blade. (a) The partition of rotating region covering the blade. (b) The grids near the blade surface.

### 3.2 Calculation conditions

In this paper, the droplet collection efficiency of blades in hovering state is carried out. And the effect of MVD on the results is mainly discussed. The calculation conditions are shown in Table 1.

Table 1 – Computational conditions

| Case | Collective pitch (°) | Angular velocity (rpm) | MVD (μm) |
|---|---|---|---|
| 1 | 12 | 140 | 20 |
| 2 | 12 | 140 | 30 |
| 3 | 12 | 140 | 40 |
| 4 | 12 | 140 | 50 |

## 3.3 Droplet collection efficiency

Fig. 2 shows the droplet collection efficiency of the blade under the condition MVD=30 μm. It can be seen that the droplet impact characteristics at the tip are significantly larger than that at the root. This is because that the droplet trajectory is affected by the velocity of the airflow and the centrifugal force. Concretely, the larger the velocity is, the greater the probability of the droplet impacting on the blade surface is. In the tip part of the blade, the velocity is greater than that in the root part, thus the droplet collection efficiency is high in blade tip. In addition, centrifugal force makes the droplet flow towards the blade tip during and after the impact, which leads a greater collection efficiency in blade tip.

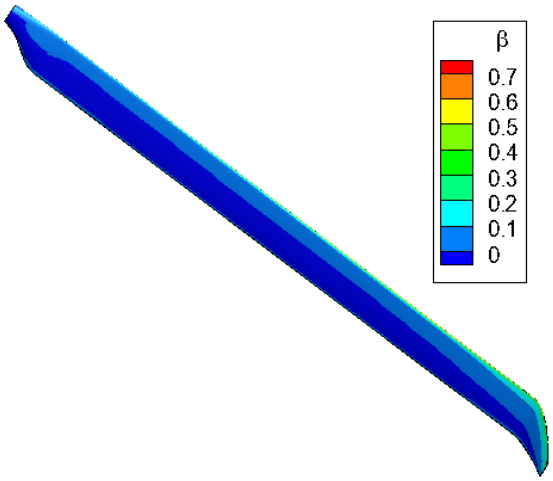


Figure 2 – Droplet collection efficiency, MVD=30 μm.

In Figure 2, we only get a qualitative result of the droplet impact. To make this understanding clear, we choose four sections and give its quantitative data. The location and coordinates of the sections 0.2R, 0.5R, 0.8R and 0.9R are given in Fig. 3(a), (b) and (c), where R is the rotor radius. And the corresponding distribution curves of droplet collection efficiency along chordal direction at four sections are also shown in Fig. 3(d). It can be seen that the droplet collection efficiency does increase gradually from root to tip under the same icing condition. The droplet collection efficiency on section 0.9R is almost 3 times of that on 0.2R.

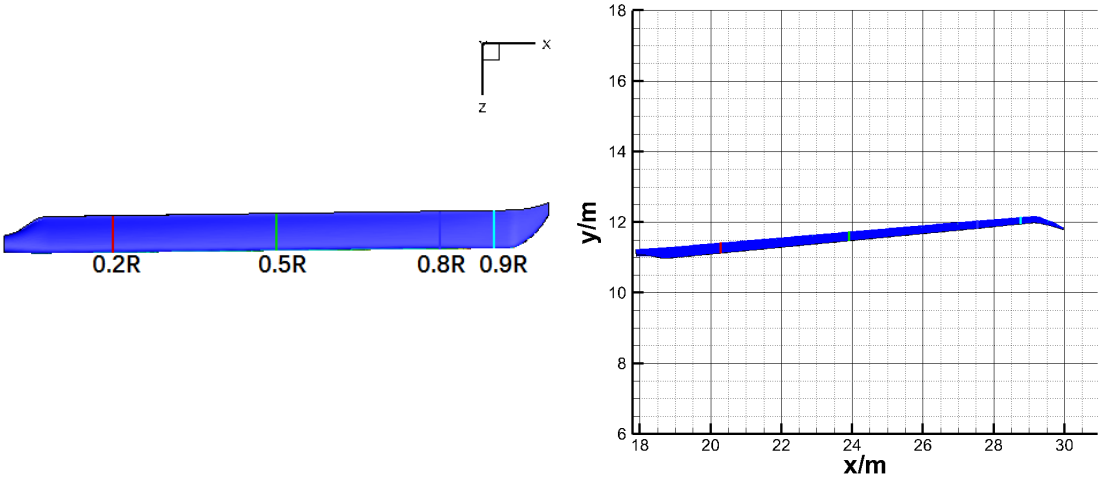


(a) (b)

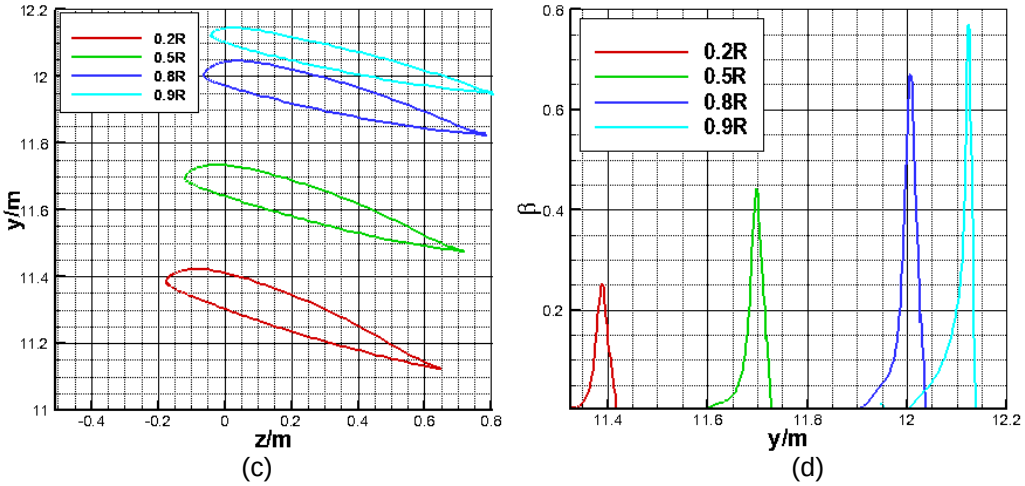


(c) (d)

Figure 3 – Droplet collection efficiency of the blade, MVD=30μm. (a) The location of four sections which are 0.2R,0.5R, 0.8R and 0.9R. (b) The coordinate of blade in X-Y plane. (c) The coordinate of four sections in Z-Y plane. (d) The curve of droplet collection efficiency on the four sections.

## 3.4 Effect of MVD on collection efficiency

The droplet collection efficiency is the key parameter to the icing, its coverage range directly show where icing appears and how serious icing is. To catch the effect of droplet MVD on icing, Figure 4 shows the droplet collection efficiency corresponding to different MVDs at the four cross sections. In these four sub-figures, we can see that the MVD has greatly affected the value of collection efficiency and range of icing. Concretely, the collection efficiency and the icing range on each cross-section in the chord direction increases along with the increase of droplet MVD. This is because that the inertia increases and the following performance of air flow becomes poor due to the mass increase of droplets, which makes the droplets easy to impact on the blades.

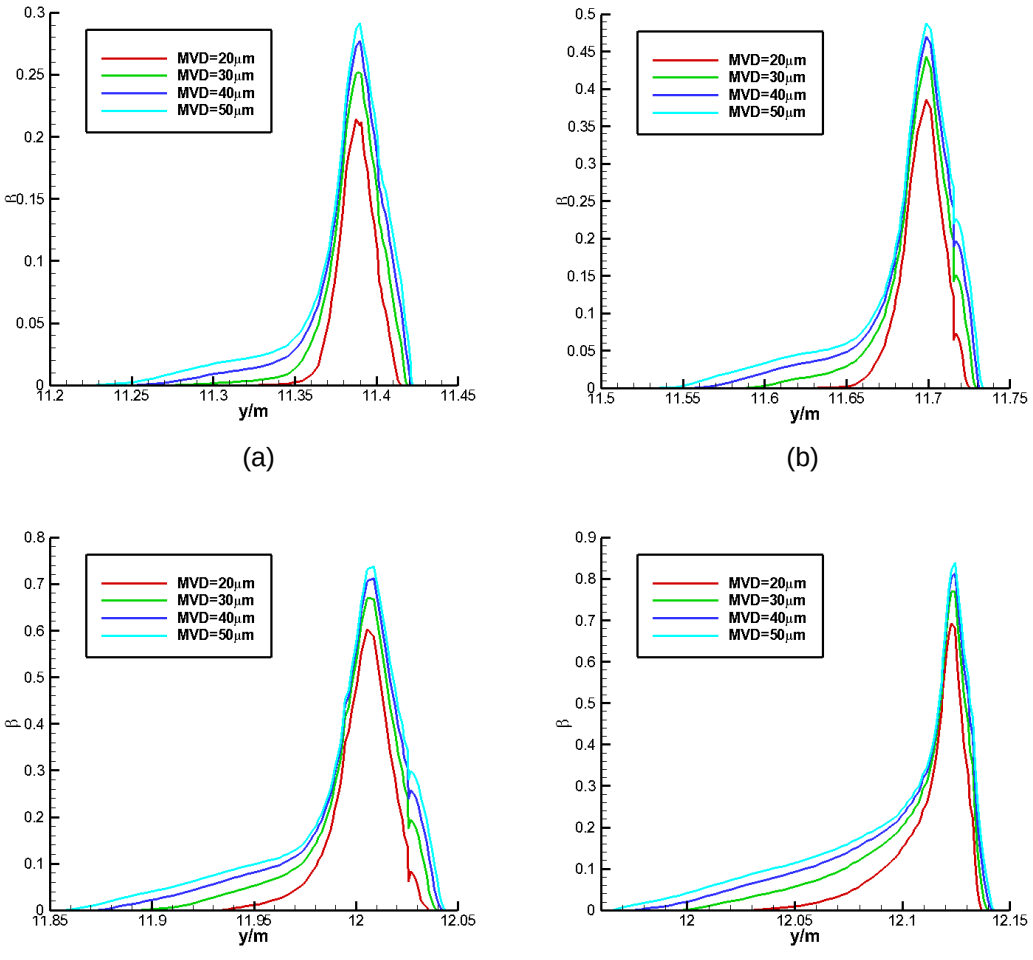


(a) (b)

(c) (d)

Figure 4 – Droplet collection efficiency on different cross-sections. (a) 0.2R. (b) 0.5R. (c) 0.8R. (d) 0.9R.

In order to make a more in-depth quantitative comparison, the maximum collection efficiencies with different MVDs on the four sections are compared in Figure 5. It can be seen that the larger the MVD is, the larger the maximum collection efficiency is. And this changing trend gradually becomes strong on the section from the root to the tip. In the 0.9R section, the difference of the maximum droplet collection efficiency under MVDs between 20 μm and 50 μm is about 0.15. Meanwhile, the section closer to the blade tip part, the greater the maximum collection efficiency for the same MVD. The maximum difference between the value on section 0.2R and 0.9R is about 0.54 when the MVD is 50 μm.

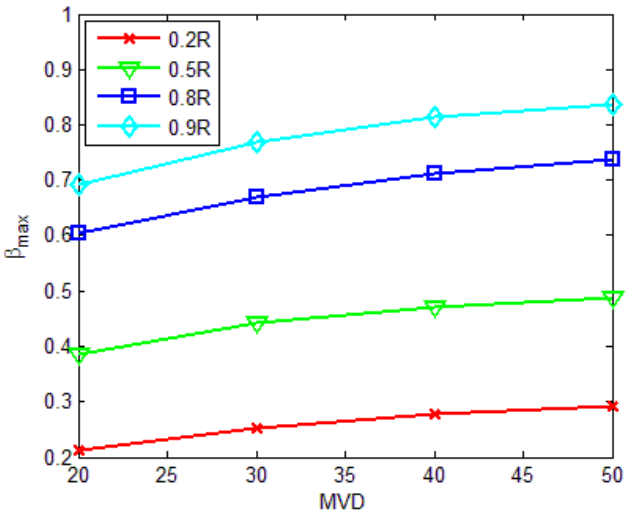


Figure 5 – Maximum value of droplet collection efficiency on different cross-sections.

In Table 2, the coverage range (where the collection efficiency $\beta > 0$) of droplets under different situations is given. The range of the upper and lower wing is computed independently and we can see that the value on the upper surface is far less than that on the lower surface, which is caused by the collection pitch of the blade. From the data in the same row, it shows that the larger the MVD is, the larger the droplet coverage range is. The coverage range under a situation of MVD 50 μm is about twice bigger than that of 20 μm. And from the data in the same column, it can also be seen that the closer section to the tip, the large the coverage range. The coverage range of the lower wing on 0.9R is about 1.6 times of that on 0.2R.

Table 2 – Coverage range of water droplets

| Location \ MVD(μm) | | 20 | 30 | 40 | 50 |
|---|---|---|---|---|---|
| 0.2R | Upper surface | 4.61% | 6.43% | 9.22% | 11.04% |
| | Lower surface | 21.24% | 31.55% | 41.75% | 51.21% |
| 0.5R | Upper surface | 4.31% | 5.86% | 7.30% | 8.49% |
| | Lower surface | 20.22% | 36.36% | 49.52% | 61.48% |
| 0.8R | Upper surface | 4.50% | 5.92% | 7.34% | 8.40% |
| | Lower surface | 24.85% | 44.62% | 57.63% | 68.28% |
| 0.9R | Upper surface | 1.77% | 2.71% | 3.54% | 4.48% |
| | Lower surface | 38.33% | 57.31% | 75.12% | 81.60% |

## 4. Conclusion

In this paper, the numerical simulation method of droplet collection efficiency on the rotor is established, and the effect of MVD on the droplet collection efficiency is analyzed. The results show that the proposed method can effectively obtain the water drop impact characteristics on the surface of the blade. Moreover, the coverage range of the droplet collection efficiency shows that the icing

range expands and the collection efficiency value increases from the root to the tip of blade. And the larger the droplet MVD, the larger the icing range and collection efficiency value.

## 5. Contact Author Email Address

Weibin Li: weibinli@cardc.cn.

## 6. Copyright Statement



## Acknowledgment:

This work was supported by the National Natural Science Foundation of China under grant no 11802327.

## Reference

[1] Taiki M, Masaya S, Makoto Y, et al. Numerical simulation of ice accretion phenomena on rotor blade of axial blower. *Journal of Thermal Science*. Vol. 21, No. 4, pp 322-326, 2012.

[2] Korkan K. Experimental study of performance degradation of a model helicopter main rotor with simulated ice shapes. *NASA-CR-190684*. 1984.

[3] Brouwers E, Palacios J, Smith E, et al. The experimental investigation of a rotor hover icing model with shedding. Phoenix: *Proceedings of American Helicopter Society 66th Annual Forum*. 2010.

[4] Liu Y, Li L, Ning Z, et al. Experimental investigation on the dynamic icing process over a rotating propeller model. *Journal of Propulsion and Power*. Vol. 34, No. 4, pp 933-946, 2018.

[5] Yihua C, Chao M, Qiang Z, et al. Numerical simulation of ice accretions on an aircraft wing. *Aerospace Science and Technology*. Vol. 23, pp 296–304, 2012.

[6] Chen N,Ji H, Hu Y, et al. Experimental study of icing accretion on a rotating conical spinner. *International Journal of Heat and Mass Transfer*. Vol. 51, No. 12, pp 1717-1729, 2015.

[7] Wang Z, Zhu C. Numerical study of atmospheric ice accretion on rotating geometric cross sections with fins. *The Journal of Computational Multiphase Flows*. Vol. 8, No. 1, pp 3-14, 2016.

[8] Yassin M, Nathoo M, Zhan Z, et al. Modeling of iced rotor dynamics via CFD-CSD coupling. Atlanta： *Applied Aerodynamics Conference*. 2018.

[9] Wang Z, Zhu C. Numerical simulation for in-cloud icing of three-dimensional wind turbine blades. *Simulation*. Vol. 94, No. 1, pp 31-41, 2018.

[10] Shu L, Li H, Hu Q, et al. Study of ice accretion feature and power characteristics of wind turbines at natural icing environment. *Cold Regions Science and Technology*. 147: 45-54, 2018.

[11] David S, Habashi W. FENSAP-ICE simulation of complex wind turbine icing events, and comparison to observed performance data. *AIAA 2014-1399*. 2014.

[12] Xi C, Qijun Z. Numerical simulations for ice accretion on rotors using new three-dimensional icing model. *Journal of Aircraft*. Vol. 54, No. 4, pp 1428-1442, 2017.

[13] Xueqin B, Guiping L, Xiaobin S, et al. Numerical simulation of aircraft thermal anti-icing system based on a tight-coupling method. *International Journal of Heat and Mass Transfer*. 148, 2020.

[14] Chen N, Du J, Ji H, et al. Numerical study of effects of centrifugal force on ice accretion on a rotor blade. *Journal of Propulsion Technology*. Vol. 41, No. 6, pp 1314-1323, 2020. (in Chinese)